UCSF

Title

Hydrogen-Bonded Water Molecules in the M2 Channel of the Influenza A Virus Guide the Binding Preferences of Ammonium-Based Inhibitors

Authors

Gianti, Eleonora
Carnevale, Vincenzo
DeGrado, William F
et al.

Hydrogen-Bonded Water Molecules in the M2 Channel of the Influenza A Virus Guide the Binding Preferences of Ammonium-Based Inhibitors

Eleonora Gianti[†], **Vincenzo Carnevale**[†], **William F. DeGrado**[‡], **Michael L. Klein**[*,†], and **Giacomo Fiorin**[†]

[†]Institute for Computational Molecular Science, Temple University, SERC Building, 1925 North 12th Street, Philadelphia, Pennsylvania 19122, United States

[‡]Department of Pharmaceutical Chemistry, University of California, San Francisco, 555 Mission Bay Boulevard South, San Francisco, California 94158, United States

Abstract
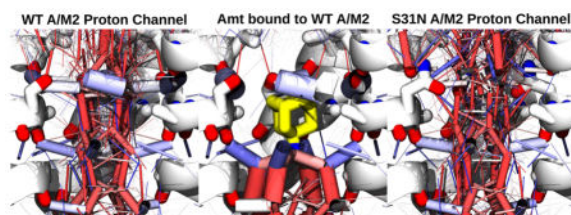
The tetrameric M2 proton channel of influenza A virus is an integral membrane protein responsible for the acidification of the viral interior. Drugs such as amantadine target the transmembrane region of wild type M2 by acting as pore blockers. However, a number of mutations affecting this domain confer drug resistance, prompting the need for alternative inhibitors. The availability of high-resolution structures of drug-bound M2, paired with computational investigations, revealed that inhibitors can bind at different sites, and provided useful insights in understanding the principles governing proton conduction. Here, we investigated by computation the energetic and geometric factors determining the relative stability of pore blockers at individual sites of different M2 strains. We found that local free energy minima along the translocation pathway of positively charged chemical species correspond to experimentally determined binding sites of inhibitors. Then, by examining the structure of water clusters hydrating each site, as well as of those displaced by binding of hydrophobic scaffolds, we predicted the binding preferences of M2 ligands. This information can be used to guide the identification of novel classes of inhibitors.

[*]Corresponding Author: mlklein@temple.edu.

1. INTRODUCTION

The conduction of protons through biological membranes is governed by competing physical and chemical factors such as the composition of the membrane, the embedded protein channels, the structural ensemble of water molecules in the regions of confinement, and the availability of titratable groups that can respond to changes in pH or relay protons themselves. The M2 channel of the influenza A virus is a 96 amino-acid tetrameric protein that balances effectively all these factors to conduct protons at a peak rate of 1000 per second.[1–3] This conduction rate is sensitive to pH, due to the presence of four histidine amino acids at position 37, approximately at the center of the a-helical transmembrane (TM) segments (Figure 1). A sustained proton flow by M2 under slightly acidic pH conditions is used to acidify the endosome that contains a viral particle after endocytosis, and to trigger the infection of a host cell.

The mechanism used by M2 to conduct protons and the strategies used to inhibit it have been studied extensively by a variety of methods, most notably electrophysiology in cells expressing M2,[2–5] neutron diffraction,[6] X-ray crystallography,[7,8] solid-state[9–12] and solution[13–17] nuclear magnetic resonance spectroscopy (NMR), and molecular simulations.[8,18–27] One of the most important findings has been the high resolution structure of the complex between M2 and its best known inhibitor, amantadine (1-adamantylamine, **Amt**) ($C_{10}H_{15}NH_3^+$).[12] M2 binds **Amt** at different binding sites:[28] a single high affinity site within the pore[12] and four low affinity sites at the interface between the channel and the lipid membrane.[14] Because the high affinity site is much less sensitive to the composition of the lipid membrane,[29,30] it offers deeper insights into the mechanism of proton conduction and a more viable approach to its inhibition.

The high affinity site can also be seen as mimicking a condition where a hydronium (H_3O^+) is replaced by a less conductible ammonium, and the TM pore is occluded by the cycloalkyl portion of **Amt**.[12] Proton influx is most likely prevented by the unavailability of water molecules in the region occupied by the cycloalkyl group (adamantane ring), which can be inferred by reasons of steric hindrance, and is also confirmed by molecular simulations.[17] The ammonium group is positioned between the backbone carbonyls of four serine amino acids at position 31, two a-helical turns before the four histidines (His37) following the direction of proton influx (Figure 1). The cycloalkyl group spans the region between the pore-lining residues 27 and the ammonium, and closely interacts with the side chains of residue 31. This position offers a straightforward explanation for the ability of certain M2 strains, containing mutations at residues 27 or 31, to maintain a decreased or intact proton influx in the presence of **Amt**.[31]

To inhibit the amantadine-resistant strains of M2, a viable strategy is to design new molecules that better adapt to a different local structure and chemical environment at the high-affinity binding site.[32] However, the availability of high-resolution structures makes it also possible to look for molecules that can bind M2 at alternative positions, while retaining the central goal of a dehydrated pore. Both strategies have been pursued with encouraging success.[15,17,33–36]

Many of the newly developed inhibitors are cycloalkyl-ammonium ions, like **Amt**. One recent class of molecules, which inhibits strains carrying the V27A mutation,[17] was designed on the basis of information from preliminary molecular dynamics (MD) simulations of the amantadine-resistant strains: in those simulations, several inhibitors including **Amt** drifted toward the histidines, leaving the outer opening of the pore fully hydrated. Molecules such as spiro-piperidine[37] or spiroadamantaneamine (**SAA**)[17] are capable of binding to wild-type M2 with the ammonium at the new position near residue 34, and V27A-M2 near residue 31 (the high affinity site of **Amt** in wild-type M2). Furthermore, molecules that feature a secondary amine connecting the adamantane group with scaffolds bearing bulky substituents are able to bind S31N-M2, the most prevalent drug-resistant mutant, by positioning the ammonium group between residues 27 and 31.[15] When analyzed together, the structures of the complexes between inhibitors of different M2 strains span three binding sites for the ammonium cation, evenly spaced alongside the helical turns of the TM domain. For ease of comparison, we number these sites counting from the N-terminal to the C-terminal end of the TM region, in ascending order with the direction of proton influx: **Site 1** represents the position between the side chains of residue 31 inside the lumen, as seen for inhibitors of S31N-M2;[15] **Site 2**, the position of the high affinity site for **Amt** in wild-type M2, is located near the carbonyl oxygen atoms of residue 31;[12] **Site 3** is situated near the carbonyl oxygen atoms of residue 34, and corresponds to the position observed for the ammonium cation of **SAA** in wild-type M2.[17] Although not observed experimentally, computational investigation indicated that **Amt** bound to S31N adopts a binding mode where the ammonium cation is shifted from its observed location in the WT lumen (**Site 2**) toward the C-terminal end of the pore,[17] and accommodates halfway between **Sites 2** and **3**, in a binding spot called **Site 3*** (refer to the Results and Discussion section for a full description).

We investigated, by computational methods, the factors determining the relative stability of each site for binding diverse ligands in different strains of M2. First, we calculated the free energy of translocation of methylammonium, the simplest molecule containing the features of M2 inhibitors, finding that the three positions described above are indeed local minima along the pathway of translocation. Second, we used the unbound protein and its S31N mutant to examine the local structure of water molecules in each of these sites, and determine the relative propensities of binding to ammonium: we found that the higher prevalence of acceptor water molecules at **Site 1** of S31N-M2 explains the activity of known inhibitors at that site particularly for this mutant but not the wild-type. Lastly, we compared the structure of the hydrophobic scaffolds of known inhibitors with the structure of water molecules displaced by them: we found that the adamantane group is a significantly good match for the water molecules of unbound wild-type M2 but not for those of the S31N mutant. The interactions between confined water molecules, the ammonium ions, and the hydrophobic scaffold can explain the principles regulating the physical mechanism of inhibition.

2. METHODS

2.1. Molecular Dynamics (MD) Simulations and Potential of Mean Force (PMF) Calculations

We used, as a model for the interaction between the protein and the drug, the TM segment of M2 (indicated as M2TM), a tetrameric bundle of α-helices spanning residues 25–46 of the protein (Udorn sequence) at the high-resolution structure solved by X-ray crystallography.[8] The four His37 side chains were initialized with a single hydrogen atom at the Nε position. Configurations of S31N-M2TM were obtained by replacing the Ser31 side chains with Asn, initialized in the same rotameric states as the NMR structure of its complex with **AIT**.[15] We embedded each protein in an 8×8 nm^2 1-palmitoyl-2-oleoylphosphatidylcholine (POPC) bilayer, hydrated by a 150 mM KCl water solution: during simulation, K$^+$ and Cl$^-$ ions did not enter the pore. We used the CHARMM36,[38,39] CGenFF,[40] and TIP3P[41] force fields for the treatment of protein and lipids, methylammonium and **Amt**, and water molecules, respectively.

We used the NAMD program[42] to perform MD simulations with a time step of 2 fs, coupled to a Langevin thermostat at a temperature of 300 K and Nosé–Hoover/Langevin barostat[43,44] at a pressure of 1 atm.

We calculated the PMFs via the metadynamics algorithm,[45] using as a variable the projection of the position of the nitrogen atom of methylammonium or **Amt** with the transmembrane axis (Figures 2 and 3). The biasing potential was composed by Gaussian hills with a magnitude of 0.001 kcal/mol and a width of 0.3 Å, added every 2 ps. We performed 200 ns-long calculations using the collective variables module of NAMD.[46]

Simulations of protein:ligand complexes were run for 65 ns, with harmonic restraints of 0.01 kcal/mol/Å^2 on (i) the protein side chains and the bound ligands and (ii) on the protein backbone. In each case, we gradually released these restraints over the first 6 and 30 ns of simulation for (i) and (ii), respectively, followed by a MD unrestrained run (Figure 4).

2.2. Populations of Hydrogen Bonds in the Binding Sites of the M2 Proton Channel

We calculated the populations of hydrogen-bonded water molecules using a clustering algorithm[47] over the frames of a MD simulation. We defined a hydrogen-bond vector between a donor and an acceptor atom when the two are at a distance less than 3.5 Å and the donor–hydrogen–acceptor angle is less than 30°. We calculated the clusters of these vectors over 50 ns-long trajectories of simulation: to define two vectors as belonging to the same cluster, we used a root-mean-square deviation (RMSD) cutoff equal to 1.5 Å. To obtain the occupancy of a hydrogen bond represented by the centroid of one cluster, we divided the population of the cluster by the total number of MD frames (thus, the occupancy of a given hydrogen bond is at most 1).

Figure 5 was produced by drawing cylinders corresponding to the centroids of each cluster, with thicknesses determined by the clusters' occupancies. Figures 1 and 5 were rendered with the VMD program.[48] The total hydrogen bond occupancy at one given site (Table 2) is given by the sum of the occupancies of all clusters whose end points are within 1.5 Å from the site's position.

2.3. Molecular Replacement of Water by Ligand Scaffolds

We calculated the electron density maps of pore ligands (Table 1) and water on a grid of resolution 0.25 Å, defined on rectangular regions centered on the channel's axis, and extending 8 Å in both directions parallel to the membrane. We chose as boundaries along the TM direction consecutive binding sites for the ammonium (labeled **Site 1**, **Site 2**, and **Site 3** as in the Introduction), as measured in Table 2. When comparing two density maps, we normalized both by dividing them by their respective integrals, to neutralize any differences arising solely from the different numbers of electrons, and to quantify instead the structural differences. We calculated the mean squared difference (MSD) between two maps, $u(\mathbf{r})$ and $w(\mathbf{r})$, by integrating $(u(\mathbf{r}) - w(\mathbf{r}))^2$ over the grid and dividing the integral by the volume of the grid. To compare the steepest varying regions of the two density maps, which correspond approximately to the molecular contours, we computed the Fourier transforms of both maps over a range of spatial frequencies starting from a chosen minimum, $1/\lambda_{cut}$. We then varied $1/\lambda_{cut}$ starting from its lowest value (given by the inverse of the smallest of the three dimensions of the grid) up to the Nyquist frequency.

3. RESULTS AND DISCUSSION

In the M2 channel, the proton conduction mechanism is guided by exchanging protons between His37 imidazole rings and waters confined to the channel's interior. Therefore, pH is a critical factor affecting conduction rates. Among the available experimental structures measured at different pH levels, the prototype for the protein/drug complex is the solid state NMR structure of A/M2-TM (Udorn strain) with bound **Amt**,[12] measured at pH 7.5. Comparisons with both the unbound X-ray structure[8] (1.65 Å), resolved at pH 6.5, and the structure of S31N-M2TM blocked by **AIT**,[15] measured at pH 6.8, show nearly identical conformations (backbone RMSD from the unbound structure of 0.7 and 1.2 Å A/M2-TM bound to **Amt** and **AIT**, respectively).[49] All of these structures are associated with a state of proton uptake, as they are "open" at the outer end and "closed" at the inner end.

Within the unifying framework of proton conduction, methylammonium cations, **Amt**, and other known M2 binders can be seen as chemical probes that selectively scan one or more "hot spots" along the channel's pore as a function of different channel mutants. We used MD simulations to define these spots as the coordinates occupied by the ammonium groups of the inhibitors listed in Table 1 in the WT or S31N M2 protein bundles. On the basis of their localization along the protonation pathway, these sites were named **Sites 1**, **2**, and **3**, including the addition of **Site 3***, counting from the N- to the C-terminal ends (center of mass of the alpha carbons for residues 25 and 46, respectively) of the M2 bundle (Figure 1), and placing the position of the center of mass of the four alpha carbons in the His37 cluster in the channel lumen as a reference system (origin of the x, y, and z axes). With the exception of **Site 3*** (which has not been measured experimentally), the position of all sites in our simulations is within one standard deviation from the experimental values.

Site 1 (average cation position 9.53 Å) is located in the N-terminal section of the pore, between Val27 and residue 31 (serine or alanine). It is shown experimentally and computationally to accommodate the positively charged moiety of **AIT** bound to the S31N mutant.[15] Our simulations indicated a similar binding mode for the weaker inhibitor **APH,**

the first benzyl-substituted amantadine derivative[33] with a slightly better potency than **Amt** against S31N while retaining (low) activity against WT (Table 1). A series of substituted amantadine derivatives of **APH** were synthesized and tested for inhibition of WT and S31N along with other mutants of the M2 channel, providing useful drug-design information through extensive structure–activity relationship studies.[33] Thus, we chose **APH** to compare with other cycloalkyl-ammonium inhibitors, due to the specific interactions formed by **AIT** with the Asn31 side chains, which increase the potency against S31N-M2 but are not conserved in WT-M2.[15]

Site 2 lies deeper in the pore (average cation position 5.11 Å), at intermediate distance between residue positions 31 and 34: it is preferred by the positively charged moiety of **Amt** in complex with the WT M2 channel.

Further down into the pore is **Site 3** (average cation position 1.99 Å). Located just above the entry cluster[8] where also Gly34 residues lie, **Site 3** stabilizes the positively charged moiety of the **SAA** bound to the WT.[17]

Lastly, one additional region, situated approximately halfway between **Site 2** and **Site 3** (average cation position 3.67 Å), accommodates the ammonium of **Amt** in complex with the S31N mutant. Given its partial overlap with **Site 3** (at distance cutoff 1.5 Å), we considered this area as an extension of the latter, and therefore, we named the former **Site 3***.

3.1. Energetics of Ammonium Cation Permeation

To model the pathway of permeation of a proton along the pore using a stable chemical analogue, we used methylammonium in lieu of a hydronium, which has a similar charge density. We then performed a similar calculation for the motion of the ammonium group of amantadine, an impermeable cation that inhibits proton conduction through the channel by occluding its pore. We measured the energetics of the pathways of permeation of these molecules by calculating PMFs based on metadynamics acting on the relative position of the nitrogen atom of the ammonium ion as a collective variable.

Permeation of positively charged moieties through the N-terminal section of the lumen of the influenza M2 channel is relatively unimpeded. The tightly packed His37 tetrad (Figure 1),[8] which endows the channel with proton selectivity, is the only structural element hindering the transit of moieties larger than a water molecule. Accordingly, the PMFs for translocation of methylammonium, calculated along the channel's axis of symmetry (z-axis), are relatively featureless for both the wild-type peptide assembly and the naturally occurring amantadine resistant mutant S31N (Figure 2).

The free energy landscape in the region adjacent to the channel's outer opening at Val27 suggests a small free energy barrier, of approximately 1 kcal/mol relatively to the exterior. This point is the major steric bottleneck along the permeation pathway toward His37, and is responsible for desolvating the cations. Within the pore, the PMF suggests a net stabilization of cations due to their interactions with bulk water molecules confined inside the lumen of M2, and thus an intrinsic ability to bind loosely positively charged molecules near the His37 tetrad (**Site 3** in Figure 2). This stabilization, observed by computational investigations from

independent groups,[18,24,50,51] can be explained by the electrostatic field generated by the phospholipid head groups, the backbone peptides in the helix bundle, and the Asp44/Arg45 dipole.[27]

Though overall lower than the bulk value, the free energy of a cation in the N-term section of the M2 pore shows interesting local variations, where discrete binding spots are apparent, all within a few kTs. These correspond to the positions along the pore's axis of the carbonyl groups of Ala30 and Gly34, and to the side chains of residue 31. Analogy with potassium channels[52,53] suggests that a "cage" of carbonyl groups at each helical turn may provide an electron rich environment able to stabilize cations, either directly or through an intervening water molecule.[8] The cations may even be either transient, as in the case of the Eigen and Zundel species of H_3O^+, or chemically stable and linked to other groups, as in the case of amino-adamantane molecules.

This picture of cation permeation as modulated by well-defined anchoring points is confirmed by the free energy profiles calculated for **Amt**. Despite the presence of a bulky adamantane group, the profile of the PMF is preserved (Figure 3): two local minima are apparent, whose positions coincide with those observed for methylammonium, although with different free energy values (Figure 2). This observation provides a strong justification for fragment-based conceptualization of ligand binding to this section of the M2 pore: the intrinsic preference for positively charged groups shown by specific regions of the pore provides, simultaneously, a set of constraints on the binding mode(s) and a "molecular ruler" to make informed guesses on the steric hindrance of the scaffold of the ligand.

Importantly, despite the fact that the positions of the binding spots for the cationic group are not perturbed by the presence of the adamantane scaffold, the relative free energy difference between **Site 1** and **Site 2** changes significantly, and **Site 2** becomes more stable than **Site 1** by approximately 5 kcal/mol in WT-M2TM (Figure 3). Thus, the net effect of the scaffold can be envisioned as a selective stabilization of one among the several minima calculated for methylammonium. In S31N-M2, the most favored minimum corresponds to **Site 1**: only one secondary minimum appears at an intermediate position between **Sites 2** and **3**, indicating the possibility of an alternative binding site, which we label as **Site 3*** (~7 kcal/mol higher than **Site 1**). No experimental structure for the complex S31N/**Amt** is currently available; nevertheless, our calculations show that, in the S31N complex, **Amt** mostly adopts a configuration with the ammonium near Val27. However, the simulation protocol does not allow for quick opening of Val27 and therefore the amantadine molecule does not leave the pore. Therefore, it is not possible to quantitatively compare minima of the WT- or S31N-M2TM PMFs as in the case of the methylammonium calculations (Figure 2), where the free energy values outside the pore were used as the zero of the free energy scale.

To confirm the predictions and understand in clearer detail the mechanism of drug binding at **Sites 2**, **3**, and **3***, we also used two ensembles of simulations with **Amt** initialized at varying positions along the pore of WT-M2 and S31N-M2 and with the ammonium oriented toward His37 (Figure 4). These show that for WT-M2 **Sites 2** and **3** are two alternative equilibria where the ammonium rapidly converges to a final position: the preference toward **Site 2** can be inferred by one simulation that spontaneously transitions from **Site 3**. For

S31N-M2, during the length of the simulations, we did not observe rotations of **Amt** from **Site 3*** to **Site 1**, and the ammonium of amantadine almost exclusively samples positions near **Site 3***. This suggest either that the free energy barrier is underestimated by the PMF (3 kcal/mol, Figure 3) or that the time scale of 65 ns (35 ns after the initial restraints on the backbone are lifted) is insufficient to capture motions of the protein backbone compared to the longer metadynamics simulations (200 ns).

3.2. Hydrogen-Bonded Water Clusters Dictate Suitable Sites for Ligand Binding

We thus proceeded to investigate the intrinsic propensity of the three sites to accommodate potential inhibitors, by examining their local structure and energetics using the unbound WT-M2 and S31N-M2.

Stabilization of Cycloalkyl-Ammonium via a Network of Hydrogen Bonds—We derived relative populations of interactions established at individual regions of the pore lumen of M2 WT and S31N mutant proton channels upon applying a clustering technique[47] that operates on hydrogen bond vectors. According to our approach, hexadimensional vectors between donor and acceptor atoms are defined for each hydrogen bond: vectors from an ensemble of simulated MD frames that are less than 1.5 Å apart belong to the same cluster. First, we extracted the position of the cations (cycloalkylammonium moieties of ligands in Table 1) as averaged over the MD trajectories of individual systems (in Table 2, these are indicated as reference M2:ligand trajectories) along the pore region (*z*-axis) of WT-M2TM and its S31N mutant. Then, for each site, we calculated the donor and acceptor occupancies as the total number of hydrogen bonds involving the cation (Table 2) within the cutoff distance. As written earlier, these are interchangeable with the corresponding experimental values (see Figure 1), only with the added information on the standard deviations.

Interestingly, comparisons with free energy profiles of the permeation pathway of ammonium cations obtained by PMFs (Figures 2 and 3) show that the sites are invariably located at local minima of the PMFs. This observation contributes strong evidence to establish their ability to be further used as binding targets for fragment- or drug-like compounds in rational design of novel inhibitors.

In addition, we extended our analysis by deriving, in every M2 channel included in this study (Table 2), the relative occupancies as the total number of atoms serving as hydrogen bond donors or acceptors at each site ("donor occupancy" and "acceptor occupancy" in Table 2).

This analysis allowed defining three possible site behaviors (Table 2), and represents a way to quickly summarize the pattern of interaction among each ligand, the water molecules in the pore, and the protein. *First*, cation stabilization sites are defined as having a high value for "donor occupancy" and an "acceptor occupancy" value close to zero. (We did not observe at any of the three sites the opposite case where the "donor occupancy" is zero but the "acceptor occupancy" is high.) *Second*, sites occupied by a nonpolar ligand moiety have both their "donor occupancy" and "acceptor occupancy" values equal to zero. *Third*,

nonzero values for both the "donor occupancy" and "acceptor occupancy" provide the signature for sites filled by clusters of hydrogen-bonded water molecules within the pore.

Interaction Pattern of Site 1—Defined as the stabilization site for the positively charged moiety of **APH** in complex with the S31N mutant (average cation position 9.53 Å), **Site 1** shows almost equivalent propensities to accommodate non-polar ligand moieties in the two unbound structures of M2. Furthermore, **Site 1** shows different distributions of hydrogen-bonded waters in the WT versus S31N structures. As a result of the replacement of a serine by an asparagine in S31N, the strong interhelix hydrogen bonds between Ser31 side chains visible as light blue cylinders in WT-M2TM (Figure 5A,B) disappear altogether (Figure 5D,E). This change results in an increase in the hydrogen-bond donor and acceptor propensities at the ammonium binding site.

Interaction Pattern of Site 2—Targeted by the positively charged substructure of **Amt** in complex with the WT channel, **Site 2** (average cation position 5.11 Å) can also offer room to accommodate the hydrophobic scaffolds of **SAA** in the case of WT-M2TM and **APH** in the case of S31N-M2TM. For this site, the populations of hydrogen-bonded waters in the two unbound structures are almost equivalent, suggesting no obvious differences in their relative stabilities.

Interaction Pattern of Site 3—Selected by the positively charged moiety of the **SAA** bound to the WT, **Site 3** (average cation position 1.99 Å) is located within 3 Å from the nitrogens of His37.[8] Analysis of the hydrogen-bond occupancies in both unbound proteins shows **Site 3** to be preferred by a donor. Localized deeper into the channel pore than all the other sites, it never accommodates a ligand moiety other than positively charged groups.

Interaction Pattern of Site 3*—Lastly, **Site 3*** represents the cation stabilization site for amantadine drug in complex with the S31N proton channel (average cation position 3.67 Å). Comparable numbers of hydrogen bonded water molecules fill **Site 3*** in unbound M2 structures. As for the WT and S31N channels in complex with a ligand other than **Amt**, we observed that **Site 3*** serves as a hydrophobic site by accommodating nonpolar chemical moieties.

3.3. Molecular Replacement of "Residual" Water Molecules

So far, our analysis allowed identifying *discrete* binding sites, namely, individual regions along the A/M2 pathway of proton conduction, which offer both energetic and geometric stabilization to ammonium cations. Interestingly, we also observed that, in the absence of a cation bound to a site, the volume inside the pore is filled with hydrogen-bonded water molecules that constitute ordered clusters (Table 2; Figure 5). Clearly, these water networks do no coordinate the cation directly, and therefore, we refer to these as "residual" water molecules. Theoretically, these could be vehicles for the conduction of protons, and hence identifying ligand moieties that can effectively displace them is of primary interest to design inhibitors of the M2 channel.

We started by computing density maps of water molecules belonging to the same hydrogen bond network along the pore. Our rationale is that a strong interaction between two connected water molecules yields a proportionally strong signal in the density map: this signal represents a pair of water molecules which could be safely displaced, because their mutual interaction dominates over the interactions with the protein's pore. We extended this working hypothesis to clusters of more than two water molecules by calculating three-dimensional density maps of all donor–acceptor pairs of water molecules in the space between a cation and the preceding TM region located toward the channel's opening valve (Val27). An exception was made for **Site 1**, which required inclusion of one additional region situated toward the histidine cluster (as shown in Figure 5G). We then compared such a map to the density of inhibitor scaffolds to evaluate their similarity in shape.

A number of computational methodologies have been previously developed to generate descriptors of molecular frameworks based on shape similarity[54–56] or volume overlap.[57] These tools have been typically developed to describe structural or topological properties of *chemical compounds*, and used in virtual screening for searching large databases of chemical structures for molecules similar to query ligands. Here, we calculated a root mean squared deviation (RMSD) between two ligand density maps by using Fourier transform with a specified cutoff to control the levels of resolution of the comparison. In the context of target validation, postprocessing in the Fourier space has been used to identify putative binding pockets in proteins.[58] Instead, thermodynamic analysis of water molecules has also been used successfully to estimate the binding free energy of given scaffolds.[59,60]

Here, we applied a relatively simple shape similarity approach to describe hydrogen-bonded *water clusters*, and to compare their maps to those generated by known M2 inhibitors. In this context, we analyzed the unbound WT and S31N M2 proton channels, and computed the electron density maps of all residual water localized in the regions adjacent to the ammonium location inside the TM segment. In addition, we computed analogous density maps for a set of molecules, including the known inhibitors **Amt**, **SAA**, and **APH** (Table 1). Then, we used individual electron density maps to derive RMSD values with hydrogen-bonded clusters of residual water molecules in the unbound proteins. We also used these mutual RMSDs as a *metric* to measure the similarity between two inhibitor molecules. In most comparisons (Figure 6), the agreement is highest (the RMSD is lowest) for a spatial frequency threshold of 0.7 Å^{-1}, which corresponds to a linear dimension of 1.43 Å, approximately the value of the van der Waals radii of the carbons. We then used the RMSD values around this spatial frequency to rank each conformation adopted by a molecule (for example, the binding mode of **Amt** against the proton channel of interest) according to the degree of similarity to a reference water structure.

Amantadine Preference for Binding Site 2 in the WT Proton Channel—We initially applied our approach to the study of the binding preferences for **Amt** toward different stabilization sites in the WT M2 and the drug-resistant S31N mutant. Our simulations showed that **Amt** presents different binding modes in the WT M2 channel versus the S31N mutant (Figures 3 and 4); this is despite the fact that the hydrophobic scaffold of **Amt** does not form specific interactions with residue 31 in either channel.

We analyzed the electron density maps of all residual water molecules localized between **Site 2** (mean position and relative standard deviation 5.11 ± 0.32 Å) and the preceding **Site 1** (9.53 ± 0.24 Å) to infer the **Amt** preferences for binding the WT channel at **Site 2** (reference binding mode in Figure 5H), ultimately achieving selective inhibition of proton conduction by occluding the pore. Indeed, by evincing a lower RMSD against the WT signature waters, we proved that the adamantane group is a better structural replacement for the hydrogen-bonded water cluster between Val27 and **Site 2** of the ammonium ion (Figure 6A). When performing this analysis on the drug-resistant mutant S31N, the mismatch between the adamantane group and the density of residual waters increases significantly. In agreement with experimental activities (Table 1), we showed that amantadine evinces a lower degree of similarity to the hydrogen-bonded water clusters of **Site 2**, and therefore constitutes a weaker structural replacement of the water clusters belonging to the unbound S31N channel (Figure 6A).

Binding Preference of APH Ammonium Cation for Site 1 of the S31N Mutant— We applied the same analysis to explain the binding mode of the poorly selective inhibitor **APH**[33] (Table 1). Our simulations suggest that the ammonium cation lies in **Site 1**, as in the experimental structure of the selective inhibitor **AIT** in complex with S31N-M2TM,[15] where the isoxazole ring forms direct hydrogen bonds with Asn31. In our simulation of **APH** in complex with S31N-M2TM, the 4-phenolic substituent positions itself similarly to the isoxazole of **AIT** (reference binding mode in Figure 5G), however without forming hydrogen bonds with Asn31. In the following, we indicate the position of the center of mass of the phenol as "**Site 0**", only to define a boundary for the density calculation (**Site 0** is *not* observed as a site for cation binding).

We computed the density map of **APH** extracted from the complex with S31N-M2TM, over the compound's docking region in the M2 channel (**Site 0**, mean position and relative standard deviation 12.5 ± 0.30 Å, to **Site 2**, 5.11 ± 0.32 Å). We then calculated relative RMSDs to compare this map with those generated for hydrogen-bonded water molecules that solvate the M2 pore areas delimited by **Site 0** to **Site 2** (Figure 6B, solid lines). To assess our similarity measure, we also plotted density RMSDs obtained for reference pairs (Figure 6B, dotted lines). We used the RMSD between **Amt** and the water cluster at **Site 1** of WT-M2TM as an example of two similar density maps (**Amt** is a strong inhibitor of WT-M2), whereas the RMSD between **Amt** and **APH** indicates density maps with low similarity.

Analysis of density RMSDs revealed that **APH** shares the same similarity level to the hydrogen-bonded water clusters in both M2 channels. The absence of a clear preference is in agreement with experimental activity data (Table 1), indicating that **APH** is a weak inhibitor of both channels (IC_{50} = 199.9 M against WT-M2, IC_{50} = 166.0 μM against S31N-M2). Although the ammonium forms specific interactions with residue 31, these do not seem sufficient to achieve high potency. The inhibitor **AIT** (IC_{50} = 16.0 μM) has additional interactions, which are provided by the isoxazole ring, which are specific for S31N-M2.[15]

Binding Preference of SAA Ammonium Cation for Site 3 of the WT—Lastly, we focused our attention on the spiroadamantane compound **SAA** (Table 1), a potent inhibitor targeting both the V27A and L26F drug-resistant mutants of M2,[17] with IC_{50} values of about 0.3 and 5.6 μM, respectively. **SAA** is also known to serve as a high micromolar range inhibitor of WT-M2 (IC_{50} = 18.7 μM), while being inactive when tested against the S31N drug-resistant mutant.

Molecular simulations of **SAA** in complex with WT-M2 and solid-state NMR experiments revealed a binding mode where the compound is shifted deeper within the pore lumen toward His37 to establish interactions via a network of water-mediated hydrogen bonds.[17] As a result, the ammonium cation of **SAA** (reference binding mode in Figure 5I) is stabilized within **Site 3** (mean position and relative standard deviation 1.99 ± 0.34 Å), leaving the remaining hydrophobic moiety filling into the space up to **Site 1** (9.53 ± 0.24 Å).

We computed density RMSDs, over the area comprised between **Site 1** and **Site 3**, for **SAA** extracted from the WT complex versus hydrogen-bonded water molecules hydrating the pore lumen of WT and S31N channels (Figure 6C). As expected for inhibitors acting in the micromolar range, the density of **SAA** is very similar to the WT-M2TM water clusters, with a profile comparable to that obtained for **Amt**. However, when plotting the density RMSD obtained against the S31N-M2TM water clusters, **SAA** retained the same degree of similarity, which does *not* explain the inactivity of this compound against S31N-M2.

To understand this limitation, we recall that strong hydrogen bonds are established between monomers of WT-M2 through its Ser31 side chains (Figure 5A and B): these interactions are absent in the corresponding region of the S31N mutant (Figure 5D and E). Superposition of the hydrophobic scaffold of **SAA** to the S31N-M2TM structure indicates that the Asn31 side chains are also unable to form hydrogen bonds with protein groups or with water. Our analysis does not capture the loss of this interaction, by using only geometric descriptors of the conformation adopted by ligand molecules or water clusters, without taking into account charge or polarity. This suggests that a good similarity between a scaffold and the water clusters within the pore is required in all proteins, but in S31N-M2 specifically, the ligand must also be a hydrogen bond partner of Asn31, as shown in the NMR structure of **AIT** within S31N-M2TM.[15]

CONCLUSIONS

We have used computational techniques to map the multiple binding sites of ammonium-based inhibitors to an important proton channel, the M2 protein of the influenza A virus. As in many computational studies of structure-driven protein/ligand binding, a prerequisite to elucidating the principles governing the formation of stable complexes is the energetics of water displacement from the binding sites.[61] This is particularly important for the M2 proton channel of the influenza A virus, where water molecules not only solvate hydrophobic regions of the protein bundle but are also the primary vehicle for proton conduction. Computational approaches can be used toward this goal not only by computing binding free energies for candidate inhibitors[25] but also by using the structure of bound water to guide the search for new scaffolds.

As shown recently by high resolution X-ray and NMR structures, three primary binding sites exist along the pore of the M2 channel, aligned with the turns of its TM helices and with the corresponding clusters of water molecules. We calculated the energetics of permeation of a cationic probe (a methylammonium molecule) along these three sites, observing that they correspond to local minima of a permeation pathway within small free energy differences. When considering a cycloalkyl-ammonium molecule with a much larger hydrophobic scaffold such as the drug amantadine, these free energy differences become much larger and ultimately render some binding sites inaccessible.

We then analyzed separately how the two primary components of each ligand (the ammonium cation and the hydrophobic scaffold) contribute to the interaction with the unbound protein at each site. We found that, prior to binding of an inhibitor, all sites are partially or fully occupied by water molecules that act primarily as hydrogen-bond donors. This is verified in both the wild-type protein (WT) and its prevalent drug-resistant mutant (S31N), with one important difference at **Site 1**, the closest to the channel's outer opening (at the N-terminal end of the TM bundle). In WT-M2, the Ser31 side chains form tight hydrogen bonds between neighboring protein monomers (shown as interhelix blue cylinders, in Figure 5A), and only a few donor water molecules are observed (the site occupancy for the apo **Site 1** is 0.06 donor atoms, in Table 2). In S31N-M2, all hydrogen bonds formed by the Asn31 side chains are with the solvent (no interhelix hydrogen bond is indeed present, Figure 5D), and many of these serve to stabilize a donor water molecule (the site occupancy for the unbound **Site 1** is 0.67 donor atoms, in Table 2, indicating a 10-fold increase over the WT).

We used this information, together with a geometric analysis, to conclude that the potency and the selectivity of an ammonium-based inhibitor are determined by its ability to (i) replace a hydrogen-bonded cluster of water molecules of similar contour and (ii) preserve any critical interaction formed by these waters with the protein. By generalizing this approach to ultimately include detailed studies of thermodynamic properties of water molecules solvating the ammonium binding sites of WT and mutant M2 channels, it can become possible to identify new scaffolds that inhibit all of the prominent strains of this viral protein.

Acknowledgments

ABBREVIATIONS

Amt amantadine

AIT thiophenyl-isoxazole-amantadine, aka M2WJ332

SAA spiroadamantane-amine

APH 4-(adaman-tan-1-yl-aminomethyl)-phenol

References

1. Pinto LH, Holsinger LJ, Lamb RA. Influenza Virus M2 Protein has Ion Channel Activity. Cell. 1992; 69(3):517–528. [PubMed: 1374685]

2. Mould JA, Li HC, Dudlak CS, Lear JD, Pekosz A, Lamb RA, Pinto LH. Mechanism for Proton Conduction of the M(2) Ion Channel of Influenza A Virus. J Biol Chem. 2000; 275(12):8592–8599. [PubMed: 10722698]

3. Mould JA, Drury JE, Frings SM, Kaupp UB, Pekosz A, Lamb RA, Pinto LH. Permeation and Activation of the M2 Ion Channel of Influenza A Virus. J Biol Chem. 2000; 275(40):31038–31050. [PubMed: 10913133]

4. Pinto LH, Dieckmann GR, Gandhi CS, Papworth CG, Braman J, Shaughnessy MA, Lear JD, Lamb RA, DeGrado WF. A Functionally Defined Model for the M-2 Proton Channel of Influenza A Virus Suggests a Mechanism for its Ion Selectivity. Proc Natl Acad Sci USA. 1997; 94(21):11301–11306. [PubMed: 9326604]

5. Ma CL, Polishchuk AL, Ohigashi Y, Stouffer AL, Schon A, Magavern E, Jing XH, Lear JD, Freire E, Lamb RA, DeGrado WF, Pinto LH. Identification of the Functional Core of the Influenza A Virus A/M2 Proton-selective Ion Channel. Proc Natl Acad Sci USA. 2009; 106(30):12283–12288. [PubMed: 19590009]

6. Duff KC, Gilchrist PJ, Saxena AM, Bradshaw JP. Neutron-Diffraction Reveals the Site of Amantadine Blockade in the Influenza-a M2 Ion-Channel. Virology. 1994; 202(1):287–293. [PubMed: 7516598]

7. Stouffer AL, Acharya R, Salom D, Levine AS, Di Costanzo L, Soto CS, Tereshko V, Nanda V, Stayrook S, DeGrado WF. Structural Basis for the Function and Inhibition of an Influenza Virus Proton Channel (vol 451, pg 596, 2008). Nature. 2008; 452(7185):380–380.

8. Acharya R, Carnevale V, Fiorin G, Levine BG, Polishchuk AL, Balannik V, Samish I, Lamb RA, Pinto LH, DeGrado WF, Klein ML. Structure and Mechanism of Proton Transport through the Transmembrane Tetrameric M2 Protein Bundle of the Influenza A Virus. Proc Natl Acad Sci USA. 2010; 107(34):15075–15080. [PubMed: 20689043]

9. Sharma M, Yi MG, Dong H, Qin HJ, Peterson E, Busath DD, Zhou HX, Cross TA. Insight into the Mechanism of the Influenza A Proton Channel from a Structure in a Lipid Bilayer. Science. 2010; 330(6003):509–512. [PubMed: 20966252]

10. Hu J, Fu R, Nishimura K, Zhang L, Zhou HX, Busath DD, Vijayvergiya V, Cross TA. Histidines, Heart of the Hydrogen Ion Channel from Influenza A Virus: Toward an Understanding of Conductance and Proton Selectivity. Proc Natl Acad Sci USA. 2006; 103(18):6865–6870. [PubMed: 16632600]

11. Hu FH, Luo WB, Hong M. Mechanisms of Proton Conduction and Gating in Influenza M2 Proton Channels from Solid-State NMR. Science. 2010; 330(6003):505–508. [PubMed: 20966251]

12. Cady SD, Schmidt-Rohr K, Wang J, Soto CS, DeGrado WF, Hong M. Structure of the Amantadine Binding Site of Influenza M2 Proton Channels in Lipid Bilayers. Nature. 2010; 463(7281):689–U127. [PubMed: 20130653]

13. Pielak RM, Schnell JR, Chou JJ. Mechanism of Drug Inhibition and Drug Resistance of Influenza A M2 Channel (vol 106, pg 7379, 2009). Proc Natl Acad Sci USA. 2009; 106(27):11425–11425.

14. Schnell JR, Chou JJ. Structure and Mechanism of the M2 Proton Channel of Influenza A virus. Nature. 2008; 451(7178):591–U12. [PubMed: 18235503]

15. Wang J, Wu YB, Ma CL, Fiorin G, Wang JZ, Pinto LH, Lamb RA, Klein ML, DeGrado WF. Structure and Inhibition of the Drug-resistant S31N Mutant of the M2 Ion Channel of Influenza A Virus. Proc Natl Acad Sci USA. 2013; 110(4):1315–1320. [PubMed: 23302696]

16. Andreas LB, Eddy MT, Chou JJ, Griffin RG. Magic-Angle-Spinning NMR of the Drug Resistant S31N M2 Proton Transporter from Influenza A. J Am Chem Soc. 2012; 134(17):7215–7218. [PubMed: 22480220]

17. Wang J, Ma CL, Fiorin G, Carnevale V, Wang T, Hu FH, Lamb RA, Pinto LH, Hong M, Kein ML, DeGrado WF. Molecular Dynamics Simulation Directed Rational Design of Inhibitors Targeting Drug-Resistant Mutants of Influenza A Virus M2. J Am Chem Soc. 2011; 133(32):12834–12841. [PubMed: 21744829]

18. Carnevale V, Fiorin G, Levine BG, DeGrado WF, Klein ML. Multiple Proton Confinement in the M2 Channel from the Influenza A Virus. J Phys Chem C. 2010; 114(48):20856–20863.

19. Khurana E, Dal Peraro M, DeVane R, Vemparala S, DeGrado WF, Klein ML. Molecular Dynamics Calculations suggest a Conduction Mechanism for the M2 Proton Channel from Influenza A Virus. Proc Natl Acad Sci USA. 2009; 106(4):1069–1074. [PubMed: 19144924]

20. Dong H, Yi M, Cross TA, Zhou HX. Ab Initio Calculations and Validation of the pH-dependent Structures of the His37-Trp41 Quartet, the Heart of Acid Activation and Proton Conductance in the M2 Protein of Influenza A Virus. Chem Sci. 2013; 4(7):2776–2787. [PubMed: 23930201]

21. Yi MG, Cross TA, Zhou HX. Conformational Heterogeneity of the M2 Proton Channel and a Structural Model for Channel Activation. Proc Natl Acad Sci USA. 2009; 106(32):13311–13316. [PubMed: 19633188]

22. Khurana E, Devane RH, Dal Peraro M, Klein ML. Computational Study of Drug Binding to the Membrane-bound Tetrameric M2 Peptide Bundle from Influenza A Virus. Biochim Biophys Acta. 2011; 1808(2):530–537. [PubMed: 20385097]

23. Yi MG, Li CG, Cross TA, Zhou HX. Molecular Dynamics Study of Amantadine Inhibition of the M2 Ion Channel of Influenza a in Phospholipid Bilayers. Biophys J. 2007:556a–556a.

24. Chen H, Wu Y, Voth GA. Proton Transport behavior through the Influenza A M2 Channel: insights from Molecular Simulation. Biophys J. 2007; 93(10):3470–3479. [PubMed: 17693473]

25. Gkeka P, Eleftheratos S, Kolocouris A, Cournia Z. Free Energy Calculations Reveal the Origin of Binding Preference for Aminoadamantane Blockers of Influenza A/M2TM Pore. J Chem Theory Comput. 2013; 9(2):1272–1281.

26. Gu RX, Liu LA, Wang YH, Xu Q, Wei DQ. Structural Comparison of the Wild-Type and Drug-Resistant Mutants of the Influenza A M2 Proton Channel by Molecular Dynamics Simulations. J Phys Chem B. 2013; 117(20):6042–6051. [PubMed: 23594107]

27. Ma CL, Fiorin G, Carnevale V, Wang J, Lamb RA, Klein ML, Wu YB, Pinto LH, DeGrado WF. Asp44 Stabilizes the Trp41 Gate of the M2 Proton Channel of Influenza A Virus. Structure. 2013; 21(11):2033–2041. [PubMed: 24139991]

28. Rosenberg MR, Casarotto MG. Coexistence of Two Adamantane Binding Sites in the Influenza A M2 Ion Channel. Proc Natl Acad Sci USA. 2010; 107(31):13866–13871. [PubMed: 20643947]

29. Cady SD, Wang J, Wu YB, DeGrado WF, Hong M. Specific Binding of Adamantane Drugs and Direction of Their Polar Amines in the Pore of the Influenza M2 Transmembrane Domain in Lipid Bilayers and Dodecylphosphocholine Micelles Determined by NMR Spectroscopy. J Am Chem Soc. 2011; 133(12):4274–4284. [PubMed: 21381693]

30. Cady S, Wang T, Hong M. Membrane-Dependent Effects of a Cytoplasmic Helix on the Structure and Drug Binding of the Influenza Virus M2 Protein. J Am Chem Soc. 2011; 133(30):11572–11579. [PubMed: 21661724]

31. Balannik V, Carnevale V, Fiorin G, Levine BG, Lamb RA, Klein ML, DeGrado WF, Pinto LH. Functional Studies and Modeling of Pore-Lining Residue Mutants of the Influenza A Virus M2 Ion Channel. Biochemistry. 2010; 49(4):696–708. [PubMed: 20028125]

32. Wang J, Ma C, Balannik V, Pinto LH, Lamb RA, DeGrado WF. Exploring the Requirements for the Hydrophobic Scaffold and Polar Amine in Inhibitors of M2 from Influenza A Virus. ACS Med Chem Lett. 2011; 2(4):307–312. [PubMed: 21691418]

33. Wang J, Ma C, Wang J, Jo H, Canturk B, Fiorin G, Pinto LH, Lamb RA, Klein ML, DeGrado WF. Discovery of novel Dual Inhibitors of the Wild-type and the most Prevalent Drug-resistant Mutant, S31N, of the M2 Proton Channel from Influenza A Virus. J Med Chem. 2013; 56(7):2804–2812. [PubMed: 23437766]

34. Eleftheratos S, Spearpoint P, Ortore G, Kolocouris A, Martinelli A, Martin S, Hay A. Interaction of Aminoadamantane Derivatives with the Influenza A Virus M2 Channel-Docking using a Pore Blocking Model. Bioorg Med Chem Lett. 2010; 20(14):4182–4187. [PubMed: 20570509]

35. Kolocouris A, Tzitzoglaki C, Johnson FB, Zell R, Wright AK, Cross TA, Tietjen I, Fedida D, Busath DD. Aminoadamantanes with Persistent in Vitro Efficacy against H1N1 (2009) Influenza A. J Med Chem. 2014; 57:4629–4639. [PubMed: 24793875]

36. Rey-Carrizo M, Barniol-Xicota M, Ma C, Frigolé-Vivas M, Torres E, Naesens L, Llabrés S, Juárez-Jiménez J, Luque FJ, DeGrado WF, Lamb RA, Pinto LH, Vázquez S. Easily Accessible

Polycyclic Amines that Inhibit the Wild-Type and Amantadine-Resistant Mutants of the M2 Channel of Influenza A Virus. J Med Chem. 2014:5738. [PubMed: 24941437]

37. Wang J, Cady SD, Balannik V, Pinto LH, DeGrado WF, Hong M. Discovery of Spiro-Piperidine Inhibitors and Their Modulation of the Dynamics of the M2 Proton Channel from Influenza A Virus. J Am Chem Soc. 2009; 131(23):8066–8076. [PubMed: 19469531]

38. MacKerell AD, Banavali N, Foloppe N. Development and Current Status of the CHARMM Force Field for Nucleic Acids. Biopolymers. 2000; 56(4):257–265. [PubMed: 11754339]

39. Klauda JB, Venable RM, Freites JA, O'Connor JW, Tobias DJ, Mondragon-Ramirez C, Vorobyov I, MacKerell AD, Pastor RW. Update of the CHARMM All-Atom Additive Force Field for Lipids: Validation on Six Lipid Types. J Phys Chem B. 2010; 114(23):7830–7843. [PubMed: 20496934]

40. Vanommeslaeghe K, Hatcher E, Acharya C, Kundu S, Zhong S, Shim J, Darian E, Guvench O, Lopes P, Vorobyov I, MacKerell AD. CHARMM General Force Field: A Force Field for Drug-Like Molecules Compatible with the CHARMM All-Atom Additive Biological Force Fields. J Comput Chem. 2010; 31(4):671–690. [PubMed: 19575467]

41. Jorgensen WL, Chandrasekhar J, Madura JD, Impey RW, Klein ML. Comparison of simple Potential Functions for Simulating Liquid Water. J Chem Phys. 1983; 79:926–935.

42. Phillips JC, Braun R, Wang W, Gumbart J, Tajkhorshid E, Villa E, Chipot C, Skeel RD, Kale L, Schulten K. Scalable Molecular Dynamics with NAMD. J Comput Chem. 2005; 26(16):1781–1802. [PubMed: 16222654]

43. Martyna GJ, Tobias DJ, Klein ML. Constant-Pressure Molecular-Dynamics Algorithms. J Chem Phys. 1994; 101(5):4177–4189.

44. Feller SE, Zhang YH, Pastor RW, Brooks BR. Constant-Pressure Molecular-Dynamics Simulation - the Langevin Piston Method. J Chem Phys. 1995; 103(11):4613–4621.

45. Laio A, Parrinello M. Escaping Free-energy Minima. Proc Natl Acad Sci USA. 2002; 99(20):12562–12566. [PubMed: 12271136]

46. Fiorin G, Klein ML, Henin J. Using Collective variables to Drive Molecular Dynamics Simulations. Mol Phys. 2013; 111(22–23):3345–3362.

47. Daura X, Gademann K, Jaun B, Seebach D, van Gunsteren WF, Mark AE. Peptide folding: When Simulation meets Experiment. Angew Chem, Int Ed. 1999; 38(1–2):236–240.

48. Humphrey W, Dalke A, Schulten K. VMD: Visual Molecular Dynamics. J Mol Graphics Modell. 1996; 14(1):33–38.

49. Fiorin G, Carnevale V, DeGrado WF. The Flu's Proton Escort. Science. 2010; 330(6003):456–458. [PubMed: 20966238]

50. Mustafa M, Henderson DJ, Busath DD. Free-energy Profiles for Ions in the Influenza M2-TMD Channel. Proteins. 2009; 76(4):794–807. [PubMed: 19296508]

51. Bankura A, Klein ML, Carnevale V. Proton Affinity of the Histidine-tryptophan Cluster Motif from the Influenza A Virus from ab initio Molecular Dynamics. Chem Phys. 2013; 422:156–164.

52. Doyle DA, Cabral JM, Pfuetzner RA, Kuo AL, Gulbis JM, Cohen SL, Chait BT, MacKinnon R. The Structure of the Potassium Channel: Molecular basis of K+ Conduction and Selectivity. Science. 1998; 280(5360):69–77. [PubMed: 9525859]

53. Roux B, MacKinnon R. The Cavity and Pore Helices the KcsA K+ Channel: Electrostatic Stabilization of Monovalent Cations. Science. 1999; 285(5424):100–102. [PubMed: 10390357]

54. Zauhar RJ, Moyna G, Tian LF, Li ZJ, Welsh WJ. Shape Signatures: A new Approach to Computer-aided Ligand- and Receptor-based Drug Design. J Med Chem. 2003; 46(26):5674–5690. [PubMed: 14667221]

55. Rush TS, Grant JA, Mosyak L, Nicholls A. A Shape-based 3-D Scaffold hopping Method and its Application to a Bacterial Protein-protein Interaction. J Med Chem. 2005; 48(5):1489–1495. [PubMed: 15743191]

56. Zauhar RJ, Gianti E, Welsh WJ. Fragment-based Shape Signatures: a new Tool for Virtual Screening and Drug Discovery. J Comput-Aided Mol Des. 2013; 27(12):1009–1036. [PubMed: 24366428]

57. Dixon SL, Smondyrev AM, Knoll EH, Rao SN, Shaw DE, Friesner R. APHASE: a new Engine for Pharmacophore Perception 3D QSAR Model Development, 3D Database Screening: 1,

Methodology and Preliminary Results. J Comput-Aided Mol Des. 2006; 20(10–11):647–671. [PubMed: 17124629]

58. Brenke R, Kozakov D, Chuang GY, Beglov D, Hall D, Landon MR, Mattos C, Vajda S. Fragment-based Identification of Druggable 'hot spots' of Proteins using Fourier Domain Correlation Techniques. Bioinformatics. 2009; 25(5):621–627. [PubMed: 19176554]

59. Young T, Abel R, Kim B, Berne BJ, Friesner RA. Motifs for Molecular Recognition Exploiting Hydrophobic Enclosure in Protein-ligand Binding. Proc Natl Acad Sci USA. 2007; 104(3):808–813. [PubMed: 17204562]

60. Ross GA, Morris GM, Biggin PC. Rapid and Accurate Prediction and Scoring of Water Molecules in Protein Binding Sites. PLoS One. 2012; 7(3)

61. Michel J, Tirado-Rives J, Jorgensen WL. Energetics of Displacing Water Molecules from Protein Binding Sites: Consequences for Ligand Optimization. J Am Chem Soc. 2009; 131(42):15403–15411. [PubMed: 19778066]
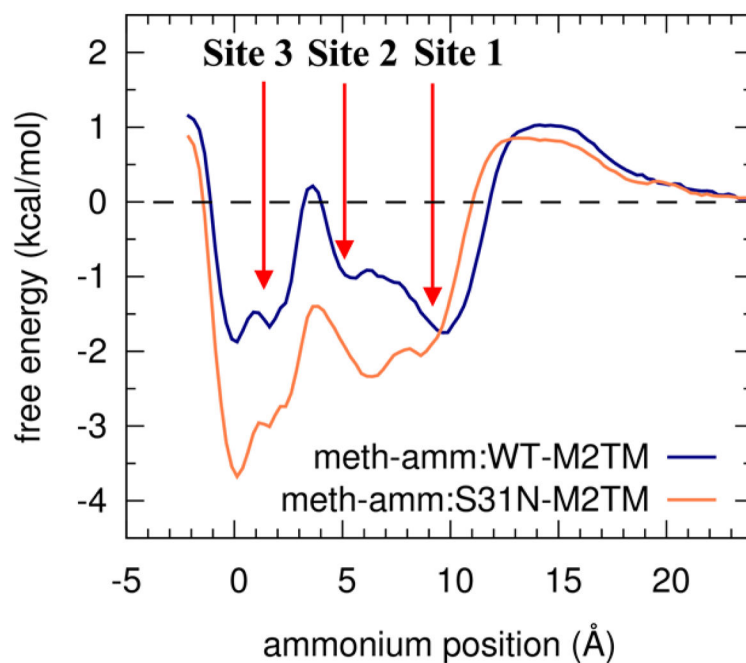
Figure 1.
Structure of the TM domain of M2:[8] shown are the pore-lining amino acids Val27, Ser31, His37, and Trp41. An asterisk marks the sites of drug-resistant mutations. Water molecules resolved crystallographically within the lumen of the protein[8] are shown as red spheres, and the backbone carbonyls interacting with them, in light blue. **Amt** is shown in pink carbons at the same position as the solid-state NMR structure of its complex with M2TM[12] and in yellow carbons from a MD simulation without experimental restraints.[17]

Figure 2.
PMFs of methylammonium ($NH_3^+CH_3$) within WT-M2TM and S31N-M2TM under high pH conditions from 200 ns simulations. Red arrows indicate the positions of the nitrogen atoms as identified in the complexes of WT-M2TM with **Amt** (**Site 2**)[12] and **SAA** (**Site 3**)[17] and of S31N-M2TM with the secondary amine derivatives of **AIT** (**Site 1**).[15] The dashed line indicates the reference free energy values observed in the bulk water solution (0 kcal/mol). On the horizontal axis, 0 Å indicates the center of mass of the four His37 alpha carbons; Val27 is found approximately at 14 Å.
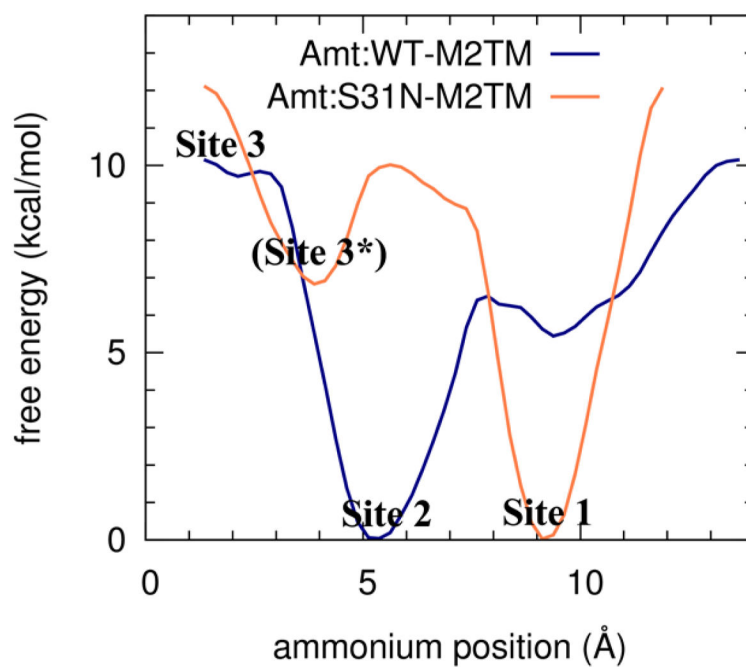
Figure 3.
PMFs for the ammonium group of **Amt** within wild-type and S31N-M2TM under high pH conditions from 200 ns MD simulations. **Amt** does not leave the pore within both simulations (ammonium position <13 Å); thus, the zero of the free energy axis is set at the global minimum of each PMF.
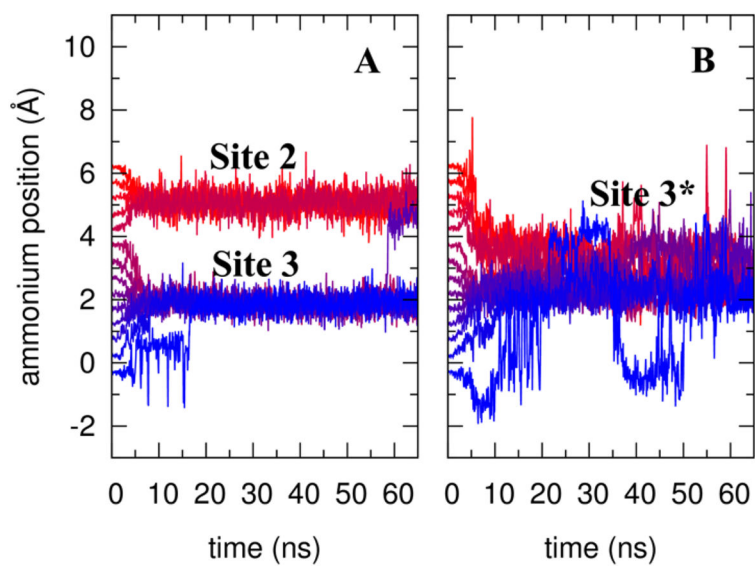
Figure 4.
Shown are the positions of the amantadine ammonium as a function of time within the pore of WT-M2TM (A) and within S31N-M2TM (B).
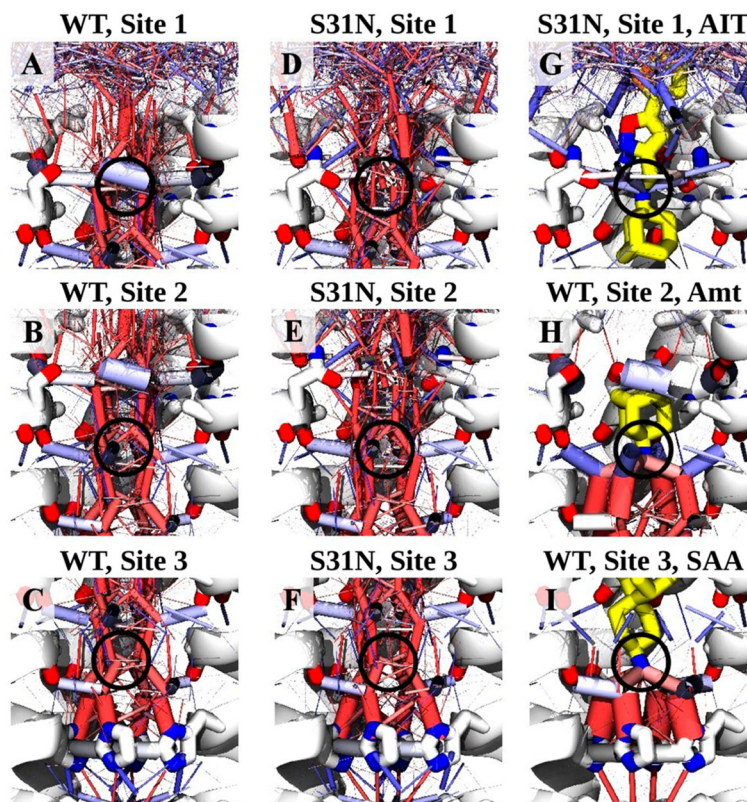
Figure 5.
Hydration of the binding sites for inhibitors of M2. (A–C) Hydrogen bond vectors in unbound WT-M2TM, recorded over 50 ns of MD simulation at **Sites 1** (A), **2** (B), and **3** (C). The protein's heavy atoms are shown as in Figure 1. Hydrogen bond vectors are shown as sticks, with thicknesses proportional to their occupancy, and colored on a scale ranging from red to blue according to the relative position of the donor and acceptor (red indicates hydrogen bonds oriented toward H37, blue in the opposite direction). (D–F) Hydrogen bond vectors in unbound S31N-M2TM for **Sites 1** (D), **2** (E), and **3** (F). (G–I) Hydrogen bond vectors in complexes with three of the inhibitors listed in Table 1: **AIT**, bound at **Site 1** to S31N (G); **Amt**, bound at **Site 2** to WT (H); and **SAA**, bound at **Site 3** to WT (I). Black circles indicate regions within a cutoff distance of 1.5 Å from each ammonium site used to calculate the hydrogen bond occupancies in Table 2.
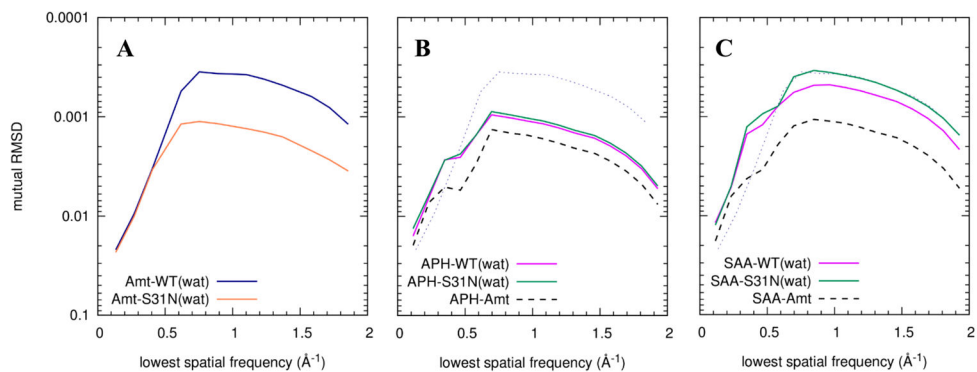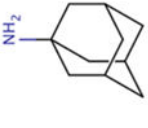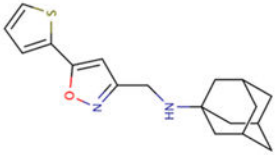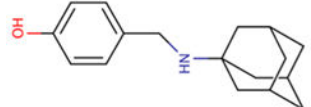
Figure 6.
Root mean squared deviations (RMSDs) between densities of bound inhibitors (see Table 1) and the densities of hydrogen-bonded water molecules within the unbound protein near each site. A "high-pass" filter is applied to all densities by removing all Fourier terms below a predefined spatial frequency (see Methods): the leftmost points of each curve (lowest spatial frequencies) correspond to RMSD calculations without any filter. (A) RMSDs between **Amt** (ammonium position at **Site 2**) and water in the region between **Site 1** (mean position and relative standard deviation 9.53 ± 0.24 Å) and **Site 2** (5.11 ± 0.32 Å) in WT- and S31N-M2TM; the RMSDs between **Amt** and WT-M2 are also shown as a dotted line in parts B and C for comparison. (B) RMSD between **APH** (ammonium position at **Site 1**) and water in the region between **Site 0** (12.5 ± 0.30 Å) and **Site 2** (5.11 ± 0.32 Å); the black dashed line indicates the RMSD between the **Amt** and **APH** molecules. (C) RMSDs between **SAA** (ammonium position at **Site 3**) and water in the region between **Site 1** and **Site 3**.

Author Manuscript   Author Manuscript   Author Manuscript   Author Manuscript

Table 1

Known Inhibitors of Wild-Type and S31N-M2 Proton Channel with Relative Activities, Indicated as Half Maximal Inhibitory Concentrations (IC$_{50}$'s, μM)[a]

Ligand acronym	Chemical structure	WT-M2		S31N-M2	
		IC$_{50}$(μM)	Cation site	IC$_{50}$(μM)	Cation site
Amt		15.7	**Site 2**	>200	*n.d.*
SAA (Cpd 9)[17]		18.7	**Site 3**	*n.d.*	*n.d.*
AIT (M2WJ332)[15]		>600	*n.d.*	16.0	**Site 1**

Ligand acronym	Chemical structure	WT-M2		S31N-M2	
		IC$_{50}$(μM)	Cation site	IC$_{50}$(μM)	Cation site
APH (Cpd 20)[33]		199.9	n.d.	166.0	n.d.

[a] **Amt**, amantadine; **AIT**, thiophenyl-isoxazole-amantadine, aka **M2WJ332**;[15] **SAA**, spiroadamantane-amine;[17] **APH**, 4-(adamantan-1-yl-aminomethyl)–phenol;[33] *n.d.*, not determined experimentally. In parentheses are their names in the corresponding articles. Activities for **Amt** in S31N-M2 and **AIT** in WT-M2 are extrapolated from percentages of inhibition.

Table 2

Relative Coordinates and Hydrogen-Bond Occupancies of Energetically Preferred Sites for Positively Charged Moieties along the M2 Pore Channel[a]

site	M2 channel	ligand name	average ammonium position (Å) (z-axis)	SD ammonium position (Å) (z-axis)	site occupancy donors	site occupancy acceptors
1	S31N	**APH**	9.53	0.24	1.37	0.00
		Amt			0.00	0.00
		n.a.			0.67	0.56
	WT	**Amt**			0.00	0.00
		n.a.			0.06	0.03
		SAA			0.00	0.00
2	WT	**Amt**	5.11	0.32	1.97	0.00
	S31N	**Amt**			0.12	0.00
		APH			0.00	0.00
		n.a.			0.11	0.14
	WT	*n.a.*			0.10	0.18
		SAA			0.00	0.00
3	WT	**SAA**	1.99	0.34	2.10	0.00
	S31N	**Amt**			0.39	0.13
		APH			2.12	0.51
		n.a.			1.54	0.66
	WT	**Amt**			0.70	0.48
		n.a.			1.79	1.28
3*	S31N	**Amt**	3.67	0.43	2.58	0.00
		APH			0.00	0.00
		n.a.			0.51	0.15
	WT	**Amt**			1.97	0.08
		n.a.			0.35	0.12
		SAA			0.05	0.00

[a]Distances are measured on the basis of the position of the center of mass of His37 (alpha carbons) in the channel lumen as a reference system (origin of the x, y, and z axes). The average and standard deviation (SD) of the ammonium's position for individual sites in different M2 channels are extracted from reference M2:ligand trajectories: **APH** in the S31N (ammonium up orientation, similarly to **AIT**), for **Site 1**; **Amt** in the WT (ammonium down orientation), for **Site 2**; **SAA** in the WT in the S31N, for **Site 3**; **Amt** in the S31N, for **Site 3*** (ammonium orientation not experimentally observed). Site occupancies are given as the total number of hydrogen-bond donor or acceptor atoms, respectively; occupancies are listed in the last two columns for all simulations, including those obtained from reference M2:ligand trajectories and from additional complexes (i.e., for each site, WT or S31N channels in complex with **APH**, **Amt**, **Amt**, **SAA** or no ligand). In the ligand name column, *n.a.* stands for "not available", meaning that no ligand is present at that particular site. Ammonium up or down indicates an orientation towards the N- or C-terminal of the TM segment, respectively.